Slowly accreting ice due to supercooled water impacting on a cold surface

T. G. Myers[a)]
Dept of Mathematics and Applied Mathematics, University of Cape Town, Private Bag, Rondebosch 7701, South Africa

J. P. F. Charpin and C. P. Thompson
Applied Mathematics and Computing Group Cranfield University, Cranfield, MK43 0AL, United Kingdom

(Received 17 July 2000; accepted 10 August 2001)

A theoretical model for ice growth due to droplets of supercooled fluid impacting on a subzero substrate is presented. In cold conditions rime (dry) ice forms and the problem reduces to solving a simple mass balance. In milder conditions glaze (wet) ice forms. The problem is then governed by coupled mass and energy balances, which determine the ice height and water layer thickness. The model is valid for ''thin'' water layers, such that lubrication theory may be applied and the Peclet number is small; it is applicable to ice accretion on stationary and moving structures. A number of analytical solutions are presented. Two- and three-dimensional numerical schemes are also presented, to solve the water flow equation, these employ a flux-limiting scheme to accurately model the capillary ridge at the leading edge of the flow. The method is then extended to incorporate ice accretion. Numerical results are presented for ice growth and water flow driven by gravity, surface tension, and a constant air shear. © *2002 American Institute of Physics.*
[DOI: 10.1063/1.1416186]

I. INTRODUCTION

Ice accretion on surfaces is a source of concern for a number of industries. Power cables and radio masts have been damaged or destroyed on numerous occasions due to the added burden of the ice or an increase in aerodynamic interaction leading to unacceptable movement such as galloping.[1–3] The effort in Canada, in particular, has been focused after the ''Great Ice Storm'' of 1998, which caused billions of dollars worth of damage to electrical equipment.[3,4] On aircraft various in-flight incidents have been shown to be directly attributable to ice accretion. This may be due to ice build-up on an aerofoil leading edge; for example, an accretion of only 0.4 mm on a wing upper surface may reduce lift by 25% and decrease the stall angle of attack by 6°.[5] Alternatively, ice may build-up on a noncritical surface and subsequently break off, damaging downstream components.[6,7] For these reasons most commercial and military aircraft are fitted with anti- and de-icing equipment. However, these devices require design compromises, they also use a considerable amount of energy; a typical system for a long range passenger jet consumes of the order 10^5 W when active. Ice accretion is also a concern for the shipping industry. Lozowski *et al.*[8] assert that marine icing is the primogenitor of icing problems, having caused grief for mariners long before aircraft or power cables were even invented.

Ice growth on aircraft and structures is primarily due to the impact of supercooled water droplets on a cold surface. Two basic types of ice may form; rime or glaze. Rime ice is associated with small droplets and very cold conditions, typically when the ambient temperature is below $-15\,°C$, so the impacting droplets freeze almost instantaneously. In milder conditions or when the water droplets are large, glaze ice forms. In this case only a fraction of the droplet will freeze instantaneously, the rest of the droplet can remain liquid for some time and may flow as ''runback'' water.

In the case of aircraft icing a number of commercial codes have been developed in order to understand and so control the problem, such as TRAJICE,[9] ONERA,[10] and LEWICE.[11] These codes involve two major components: the air flow and associated droplet trajectories and the icing calculation. The air and droplet flow provides the *catch* (the rate at which droplets impact at a given region) and is relatively well understood. Since rime ice formation involves no water flow on the aircraft surface, rime ice thickness is proportional to the catch and current aircraft icing codes can provide good agreement with experimental data. When glaze ice forms, the water flow can significantly complicate the issue and none of the present codes are able to deal with this. This has recently been pointed out by Bourgault *et al.*[12] who describe a limitation of conventional icing codes as ''the very crude geometric modeling of the water film.'' It was also highlighted in a collaborative study[13] between the US, UK, and France which compared the respective nations' icing codes. The current work is therefore an attempt to develop a theoretical model for the problem of ice accretion in the presence of a flowing water film. The original motivation for the work is aircraft icing (a version of the model is currently being employed in a commercial aircraft icing code ''ICECREMO,'' [7,14] see the Acknowledgments). However, the models are applicable to ice growth on any cold structure. In particular, ice accretion on a wind turbine occurs in an identical manner to that on aircraft, although the wind

a)Author to whom correspondence should be addressed. Electronic mail: myers@maths.uct.ac.za

speeds are typically lower.[3,15] Ice build-up on power lines and related equipment also occurs as a result of in-cloud icing or freezing rain and drizzle.[1,3,4] In a wider context, solidification from a flowing liquid or a droplet spray is of interest in the casting of metals and spray forming, lava flows and hydrate build-up in oil pipelines.[16–19] The question of how to determine model inputs, such as the air flow and droplet trajectories will not be addressed in the current work, since these are viewed as part of the outer solution. Further information on this aspect may be found in Refs. 1, 3, 7, and 8, for example.

The model developed in this paper involves a supercooled fluid impacting with a surface which is below 0 °C. One important model assumption is that the ice accretes slowly and with a very thin water layer, such that the dominant mechanism for heat transfer is conduction. The analysis carried out later in this paper shows that the Peclet number is indeed small for the flows of interest. This means that the assumption that the fluid is at the liquidus, which is frequently employed to analyze phase change problems with flow, is not necessary.[16,19,20]

The solidification will be treated by solving heat equations in the solid and fluid and then using this information in an energy balance. The fluid will be treated as a thin, continuous film. Under certain conditions ice accretions will exhibit sufficiently severe surface roughness for the film to break up and so the roughness elements may be partially dry. In this case the film should be considered as an average quantity over an area encompassing both wet and dry regions. The roughness will play a role by affecting not only the film height but also the ease with which the fluid moves over the surface. This average approach has been successfully applied to water flow over very rough surfaces of partially inundated soil.[21] Poots[1] (and references therein) describes the use of film flow models on accreting ice surfaces and demonstrates the validity of this approach by comparison with experiments. Bourgault *et al.*[12] have applied a simple film flow model to the problem of aircraft icing. The effect of surface roughness on the heat transfer coefficient and current practice in icing codes is discussed in Gent *et al.*

A significant difference between the current work and previous models of phase change with flow is that standard models involve substances whose physical properties, such as density, specific heat, and conductivity remain constant through the phase change, allowing a number of simplifications to be made. For the current problem this is not the case, for example, the specific heat of glaze ice is half the value of water, and so in the current work the physical properties are allowed to switch through the phase change. Rime ice density is slightly lower than glaze ice, 880 and 917 kg/m^3, respectively. Since the variation is relatively small the average value, $\rho_i = 898\ \mathrm{kg/m^3}$ will be used throughout this work. Although it is relatively simple to relax this restriction and use separate values for the two cases.[22]

In the following section the mathematical model is developed. The water flow is considered in Sec. II A; lubrication theory is employed to simplify the governing equations. Ignoring the coupling with the ice accretion, the equation which results is typical of thin film free surface flows.[23] The thermal problem requires solving heat equations in the ice and water layers with energy conservation across the phase change interface. This is dealt with in Sec. II B. In Sec. III A the one-dimensional model is discussed. This is relatively simple and has been dealt with in previous publications,[22,24] however, it provides valuable insight into the subsequent two- and three-dimensional work. Perhaps the most difficult aspect of the current work is modelling the water flow, particularly in the vicinity of the moving contact line, this has been the subject of intensive investigation for many years.[23,25–27] The numerical method employed to solve the water flow equations is described in Sec. IV. Finally, the combined ice growth and water flow is dealt with in Sec. V.

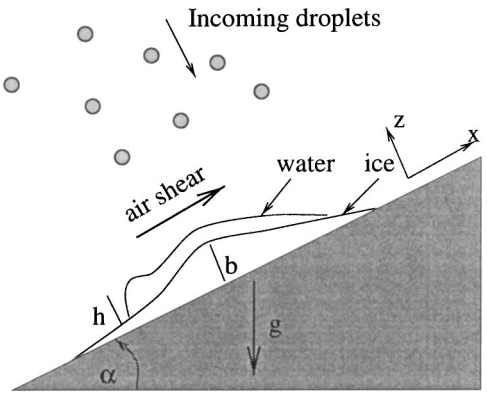

FIG. 1. Problem configuration.

II. MATHEMATICAL MODEL

The model configuration is shown in Fig. 1, which is a typical cross section of an ice and water accretion. The x and y axes define the substrate, the z axis points away from the substrate. In the 2D calculations of Secs. IV A and V A the coordinates employed are x and z. Throughout the following work the ice height will be denoted by b, the thickness of the water layer on top of the ice is h. The temperature in the ice and water is denoted T and θ, respectively.

A. Fluid flow

The fluid flow model requires the following assumptions:

(1) The effect of temperature on the viscosity, μ_w, and density, ρ_w, of the fluid is relatively small until the sudden change as solidification occurs, therefore, for the flow calculation μ_w and ρ_w are taken as constant.
(2) The aspect ratio of the flow, ϵ, and reduced Reynolds number, $\epsilon^2\,\mathrm{Re}$, are both sufficiently small that lubrication theory may be applied (this assumption is shown to be appropriate in Sec. II C).

Assumption (1) means that the fluid is incompressible and the flow effectively decouples from the thermal problem, together with assumption (2) this reduces the Navier–Stokes and continuity equations to

$$\mu_w \frac{\partial^2 u}{\partial z^2} = \frac{\partial p}{\partial x} - \rho_w g \hat{\mathbf{g}} \cdot \hat{\mathbf{x}} + \mathcal{O}(\epsilon^2, \epsilon^2 \mathrm{Re}), \tag{1}$$

$$\mu_w \frac{\partial^2 v}{\partial z^2} = \frac{\partial p}{\partial y} - \rho_w g \hat{\mathbf{g}} \cdot \hat{\mathbf{y}} + \mathcal{O}(\epsilon^2, \epsilon^2 \mathrm{Re}), \tag{2}$$

$$0 = \frac{\partial p}{\partial z} - \rho_w g \hat{\mathbf{g}} \cdot \hat{\mathbf{z}} + \mathcal{O}(\epsilon^2, \epsilon^2 \mathrm{Re}), \tag{3}$$

$$\boldsymbol{\nabla} \cdot \mathbf{u} = 0, \tag{4}$$

where $\mathbf{u}=(u,v,w)$ denotes the fluid velocity and p is the fluid pressure. These require solving subject to no-slip at the ice-water interface, $z=b$:

$$\mathbf{u} \cdot \hat{\mathbf{t}}_x = \mathbf{u} \cdot \hat{\mathbf{t}}_y = 0, \tag{5}$$

where $\hat{\mathbf{t}}_x$ and $\hat{\mathbf{t}}_y$ are the unit tangent vectors on the ice surface whose main component is in the x and y directions. Consistent with the lubrication assumption, the leading order form of this boundary condition is

$$u = v = \mathcal{O}(\epsilon^2). \tag{6}$$

Continuity of mass flux provides another condition at $z=b$:

$$\rho_w \mathbf{n} \cdot (\mathbf{u} - \mathbf{u}_b) = \rho_i \mathbf{n} \cdot (\mathbf{u}_s - \mathbf{u}_b), \tag{7}$$

where $\mathbf{u_b}=(0,0,\partial b/\partial t)$ is the velocity of the boundary and $\mathbf{u_s}=\mathbf{0}$ is the velocity of the ice, the normal $\mathbf{n}=(-\partial b/\partial x, -\partial b/\partial y, 1)$. Expanding (7) and applying (6) leads to

$$w = \left(1 - \frac{\rho_i}{\rho_w}\right) \frac{\partial b}{\partial t}, \tag{8}$$

where ρ_i and ρ_w are the density of the ice and water, respectively. Note, this implies that if $\rho_i = \rho_w$ then $w=0$ and there is no normal fluid motion at the interface. Normal motion only occurs if there is a mismatch in density between the phases forcing movement to accommodate new ice.

A similar condition to (7) is imposed at the water–air interface, $z=b+h$. In this case the boundary velocity $\mathbf{u_b} = [0,0,(\partial b/\partial t)+(\partial h/\partial t)]$. The water droplets are assumed to impact vertically with a constant velocity. The appropriate density to replace ρ_i in (7) is that of the droplet content of the air, ρ_A, where $\rho_A \ll \rho_w$. This leads to

$$w = \left(1 - \frac{\rho_A}{\rho_w}\right)\left(\frac{\partial b}{\partial t} + \frac{\partial h}{\partial t}\right) + u\left(\frac{\partial b}{\partial x} + \frac{\partial h}{\partial x}\right) + v\left(\frac{\partial b}{\partial y} + \frac{\partial h}{\partial y}\right) - \frac{\rho_A}{\rho_w}\beta W, \tag{9}$$

at $z=b+h$. The density of the air/droplet mixture is significantly less than the water density, $\rho_A/\rho_w \ll 1$, and so will be neglected in the first term on the right-hand side of (9). The product βW represents the catch efficiency, β, multiplied by the free stream velocity, W. On an accreting ice surface the catch varies with both position and time, $\beta = \beta(x,y,t)$. Typically $W \sim \mathcal{O}(10^2)$ m/s, $\beta \in [0,1]$ and so the final term in (9) will be retained. Continuity of shear and normal stress at the water–air interface, leads to

$$\mu_w \frac{\partial u}{\partial z} = A_1 + \mathcal{O}(\epsilon^2), \quad \mu_w \frac{\partial v}{\partial z} = A_2 + \mathcal{O}(\epsilon^2), \tag{10}$$

$$p - p_a = -\sigma \boldsymbol{\nabla}^2 (b+h) + \mathcal{O}(\epsilon^2), \tag{11}$$

where (A_1, A_2) are the components of shear due to the air flow, they may vary with x, y and t, σ is the surface tension. A detailed analysis concerning the coupling between the air and water flow is not carried out in the current work, for further information on this subject the reader is referred to Craik,[28] King *et al.*,[29] Tsao *et al.*,[30] and Yih.[31] Provided the water velocity is significantly less than the free stream velocity, within the current level of approximation it is sufficient to assume the shear stress caused by the air is the same as that which would occur on a dry surface.[12,32] This is termed the primary flow by Yih.[31] The curvature term in (11), which determines the magnitude of the surface tension induced stress, has been approximated to be consistent with lubrication theory. The total curvature comprises the sum of the curvatures of the ice and water surfaces. In this way the shape of the ice accretion affects the fluid motion. This effect has previously been noted in studies of flow on curved surfaces,[33,34] where it is termed an "overpressure."

The fluid pressure may be determined immediately by integrating (3) subject to (11):

$$p - p_a = \rho_w g \hat{\mathbf{g}} \cdot \hat{\mathbf{z}} (z-h) - \sigma \boldsymbol{\nabla}^2 (b+h). \tag{12}$$

Integrating (1) and (2) subject to (6) and (10) gives the fluid velocities:

$$\mu_w u = \frac{1}{2}\left(\frac{\partial p}{\partial x} - \rho_w g \hat{\mathbf{g}} \cdot \hat{\mathbf{x}}\right)(z^2 - b^2 - 2(z-b)(b+h)) + A_1(z-b), \tag{13}$$

$$\mu_w v = \frac{1}{2}\left(\frac{\partial p}{\partial y} - \rho_w g \hat{\mathbf{g}} \cdot \hat{\mathbf{y}}\right)(z^2 - b^2 - 2(z-b)(b+h)) + A_2(z-b). \tag{14}$$

Integrating the continuity equation (4) across the film gives

$$w|_{b+h} - w|_b = -\int_b^{b+h} \left(\frac{\partial u}{\partial x} + \frac{\partial v}{\partial y}\right) dz. \tag{15}$$

Applying Leibniz' theorem and substituting for w via (8) and (9) leads to the mass balance

$$\frac{\partial h}{\partial t} + \boldsymbol{\nabla} \cdot \mathbf{Q} = \frac{\rho_A}{\rho_w}\beta W - \frac{\rho_i}{\rho_w}\frac{\partial b}{\partial t}, \tag{16}$$

where the fluid flux

$$\mathbf{Q} = \left(-\frac{h^3}{3\mu_w}\left(\frac{\partial p}{\partial x} + G_1\right) + \frac{h^2}{2\mu_w}A_1, -\frac{h^3}{3\mu_w}\left(\frac{\partial p}{\partial y} + G_2\right) + \frac{h^2}{2\mu_w}A_2\right), \tag{17}$$

where $(G_1, G_2, G_3) = \rho_w g (\hat{\mathbf{g}} \cdot \hat{\mathbf{x}}, \hat{\mathbf{g}} \cdot \hat{\mathbf{y}}, \hat{\mathbf{g}} \cdot \hat{\mathbf{z}})$.

Equation (16) is a fourth-order nonlinear degenerate partial differential equation, typical of free surface flows involving surface tension. A review of similar equations may be found in Myers.[23] The constant air shear term ($\propto h^2$) may also be generated by assuming a flow driven by a constant surface tension gradient.[35,36] For structural icing gravity is typically the dominant force away from the contact line, in

aircraft icing the air shear will dominate. The final term on the right-hand side of (16) shows the ice growth rate acting as a sink for the fluid flow. This term is determined by considering the thermal problem.

B. Thermal problem

Before solving the flow equation an expression for the freezing rate, $\partial b/\partial t$, is required. This is determined by considering the thermal problem, which is governed by heat equations in the ice and water layers. The limit of particular interest to the present study is when the ice and water layers are sufficiently thin that conduction is the dominant method of heat transfer. Terms of $\mathcal{O}(\mathrm{Pe})$, where Pe is the Peclet number, will therefore be neglected; this will be discussed later. To be consistent with the preceding section, terms of $\mathcal{O}(\epsilon^2)$ will also be neglected. The heat equations then reduce to pseudosteady forms:

$$\frac{\partial^2 T}{\partial z^2} = \mathcal{O}(\epsilon^2, \mathrm{Pe}), \tag{18}$$

$$\frac{\partial^2 \theta}{\partial z^2} = \mathcal{O}(\epsilon^2, \mathrm{Pe}), \tag{19}$$

where T and θ are the ice and water temperatures, respectively. Equations (18) and (19) are solved subject to the following conditions. The ice is in perfect thermal contact with the substrate, which has high conductivity and a thermal mass much greater than that of the ice accretion:

$$T = T_s \quad \text{at } z = 0, \tag{20}$$

where T_s is the substrate temperature. It is assumed that this is the same as the ambient temperature. The temperature is continuous at the phase change boundary and equal to the freezing temperature, T_f:

$$T = \theta = T_f \quad \text{at } z = b. \tag{21}$$

In the absence of a water layer this condition is not imposed. At the air/water interface a mixed boundary condition is imposed:

$$\frac{\partial \theta}{\partial z} = q_0 + q_1 \theta \quad \text{at } z = b + h. \tag{22}$$

This general form permits the incorporation of various energy terms. For ice growth on structures q_0 represents the energy source terms, such as aerodynamic heating and kinetic energy and q_1 represents the sink terms, such as convective heat transfer and evaporation. Both q_0 and q_1 depend on the air flow and catch and therefore may vary with the surface position and time, i.e., $q_0 = q_0(x,y,t)$, $q_1 = q_1(x,y,t)$. Details on these energy terms are given in Appendix A. The heat transfer coefficient is a particularly thorny issue for icing calculations. Bourgault *et al.*[12] state that using a compressible Navier–Stokes solver to determine the outer flow solution automatically produces heat transfer coefficients. Thomas *et al.*[37] discuss heat transfer coefficient in aircraft icing conditions and provide a number of suitable references, including empirical models dealing with the effect of surface roughness. Gent *et al.*[7] discuss the methods currently employed in various commercial codes for heat transfer in laminar and turbulent flows on both smooth and rough surfaces. Other methods to estimate this quantity may be found in Poots,[1] Makkonen,[3,38] and Arnold *et al.*,[39] for example.

For rime ice the equivalent boundary condition is

$$\frac{\partial T}{\partial z} = q_{0r} + q_{1r} T \quad \text{at } z = b. \tag{23}$$

In this case the energy terms are slightly modified from the glaze ice terms. For example, the convective cooling occurs over a dry surface and evaporation is replaced by sublimation. The energy due to the latent heat release, $\rho_A \beta W L_f$, must also be included as an energy source in q_{0r}.

1. Rime ice growth

If no water layer is present, then rime ice forms. The ice thickness may be determined by integrating (16), subject to $h \equiv 0$ and $b = 0$ at $t = 0$. Since the air shear and catch may vary in time as ice accretes, in general this must be carried out numerically. However, if the ice accretion is not too large the time dependence may be neglected and

$$b = \frac{\rho_A}{\rho_i} \beta W t. \tag{24}$$

The temperature profile follows from (18) subject to (20) and (23)

$$T = T_s + \frac{q_{0r} + q_{1r} T_s}{1 - q_{1r} b} z. \tag{25}$$

These expressions for ice thickness and temperature completely solve the problem when the time variation is small. This is equivalent to a one-step solution employed in a number of icing codes. If the model inputs have a strong time dependence then the ice thickness is determined by the numerical integral of (16), the temperature profile is still determined by (25).

2. Glaze ice growth

If a water layer exists, the leading order temperature in the ice and water satisfy the quasisteady equations (18) and (19), which require solving subject to (20), (21), and (22). The temperature profiles are then given by

$$T = T_s + (T_f - T_s) \frac{z}{b}, \tag{26}$$

$$\theta = T_f + \frac{q_0 + q_1 T_f}{1 - q_1 h} (z - b). \tag{27}$$

For glaze ice growth the thermal problem is coupled to the fluid flow through the water layer thickness, h, in (27) and the ice accretion rate and thickness which appear in (16). The accretion rate is determined by considering the energy balance at the ice–water interface. Conservation of energy requires

$$[\rho_i(\mathbf{u_s} - \mathbf{u_b})\mathcal{E}_i - \rho_w(\mathbf{u} - \mathbf{u_b})\mathcal{E}_w] \cdot \mathbf{n} = [\boldsymbol{\nabla}(k_i T) - \boldsymbol{\nabla}(k_w \theta)] \cdot \mathbf{n}, \tag{28}$$

TABLE I. Typical parameter values.

b_p	5×10^{-6}	m	W	100	m/s
c_i	2030	J/kg K	β_0	0.5	
c_w	4220	J/kg K	k_i	2.18	W/mK
h_p	5×10^{-6}	m	k_w	0.571	W/mK
L_f	3.344×10^5	J/kg	μ_w	10^{-3}	Pa s
T_f	273.15	K	ρ_A	10^{-3}	kg/m^3
T_s	272.0	K	ρ_i	898	kg/m^3
A_1	0.5	Pa	ρ_w	1000	kg/m^3
A_2	0.5	Pa	σ	0.0727	N/m

where $\mathcal{E}_i$ and $\mathcal{E}_w$ are the enthalpy of the ice and water, k_i and k_w represent the thermal conductivities and the normal $\mathbf{n}$ is the same as in the preceding section. Expanding (28), with the velocities as previously specified and using Eq. (8), leads to

$$\rho_i\frac{\partial b}{\partial t}(\mathcal{E}_w-\mathcal{E}_i)=k_i\frac{\partial T}{\partial z}-k_w\frac{\partial\theta}{\partial z}-\frac{\partial b}{\partial x}\left(k_i\frac{\partial T}{\partial x}-k_w\frac{\partial\theta}{\partial x}\right)-\frac{\partial b}{\partial y}\left(k_i\frac{\partial T}{\partial y}-k_w\frac{\partial\theta}{\partial y}\right). \tag{29}$$

Finally, with the latent heat defined as the jump in enthalpy, $L_f=\mathcal{E}_w-\mathcal{E}_i$, the Stefan condition is obtained,

$$\rho_i L_f\frac{\partial b}{\partial t}=k_i\frac{\partial T}{\partial z}-k_w\frac{\partial\theta}{\partial z}+\mathcal{O}(\epsilon^2). \tag{30}$$

The temperature gradients may be determined from (26) and (27), substituting these into (30) provides the governing equation for the ice accretion:

$$\rho_i L_f\frac{\partial b}{\partial t}=k_i\frac{T_f-T_s}{b}-k_w\frac{q_0+q_1T_f}{1-q_1h}. \tag{31}$$

The glaze problem is now reduced to its final form. This involves the solution of the coupled mass and energy balances (16) and (31), which must be solved for the ice and water layer thicknesses, b and h. Once this is achieved the temperature in each layer is determined via (26) and (27). Note, this form of energy balance (31) does not preclude time variation in the model inputs, such as the energy terms, q_0 and q_1.

In its present form the mathematical description of glaze ice growth is complex, requiring the solution of coupled fourth- and first-order nonlinear partial differential equations. In particular, the mass balance (16), in the absence of ice formation, is typical of free surface thin film flows. These are notoriously difficult to solve in the vicinity of a moving contact line.[23,25–27] For this reason the numerical work of the following sections deals initially with the water flow; the complication of freezing is a relatively simple extension. However, before solving the full problem, the one-dimensional problem and various limiting cases will be considered, to provide a clearer understanding of the subsequent work and to verify the numerical solutions.

C. Justification for approximations

In deriving the system of equations governing this problem various terms have been neglected. To determine whether these approximations are justified the nondimensional numbers associated with the problem will now be evaluated. The appropriate nondimensional numbers are

$$\epsilon^2=\frac{H^2}{L^2},\quad \mathcal{A}_1=\frac{A_1H}{\mu_wU},\quad \mathcal{A}_2=\frac{A_2H}{\mu_wU},\quad C=\epsilon^3\frac{\sigma}{\mu_wU},$$

$$G=\epsilon^2\frac{\rho_wgL^2}{\mu_wU},\quad \mathrm{Pe}=\frac{\rho_Ac_i\beta_0WH}{k_i},\quad \epsilon^2\,\mathrm{Re}=\epsilon^2\frac{\rho_wUL}{\mu_w},$$

$$S=\frac{\rho_A\beta_0WHL_f}{k_i(T_f-T_s)}. \tag{32}$$

These represent the square of the aspect ratio, the ratio of the air shear to viscous forces in the x and y directions, the capillary number, the Bond number, the Peclet number, the reduced Reynolds number and the Stefan number. They involve the height and length scales H and L, the velocity scale U, the specific heat of ice, c_i, and the maximum value for the catch, β_0; all other terms have been defined previously. In all of the following examples the air shear will be set to a constant value. If it is allowed to vary then A_1 and A_2 in the above expressions should be replaced by their maximum values. Similarly β will be assumed to vary only in space, so β_0 represents the maximum value of β throughout the calculation.

Typical values for the physical constants required in (32) are given in Table I. These values are appropriate for ice and water accretion under general conditions, except for W. In aircraft icing a typical value for the wind velocity is 100 m/s. On a static structure the wind speed will be significantly lower, providing a typical value $W=\mathcal{O}(20)$ m/s. In this case the ice will accrete more slowly; this will strengthen the validity of the approximations. In the following work the extreme value, $W=100$ m/s will be used. The substrate temperature T_s is assumed to be the same as the air temperature. Further information on appropriate values for the physical constants may be found in Poots,[1] Myers,[22] Myers and Hammond.[24]

A typical height-scale for a water film on an aircraft is $H\sim10^{-4}$ m (this is confirmed by the numerical results of Sec. IV). The focus of the present analysis is on systems where the time scale, τ, is determined by the rate at which mass enters the system,

$$\tau=\frac{\rho_iH}{\rho_A\beta_0W}. \tag{33}$$

This gives a time scale $\tau \approx 2$ s. The reference density in (33) has been chosen as the ice density although the water density would work equally well, since the values only differ by approximately 10%. This time scale will be appropriate for situations where conduction is the dominant method of heat transport. The same time scale was used in a study of one-dimensional ice and water layer growth.[24] Assuming air shear is the dominant driving force, $U = A_1 H/\mu_w \approx 0.05$ m/s and the length scale $L = U\tau = 0.1$ m. The nondimensional numbers may now be calculated,

$$\epsilon^2 \approx 10^{-6}, \quad C \approx 10^{-6}, \quad G \approx 1, \quad \mathrm{Pe} \approx 5 \times 10^{-3},$$

$$\epsilon^2\,\mathrm{Re} \approx 5 \times 10^{-3}, \quad S \approx 0.75.$$

The size of these numbers justifies the approximations made during the model derivation. The smallness of the reduced Reynolds number and ϵ^2 indicates that the use of lubrication theory is appropriate. The Peclet number is small, indicating that conduction is the dominant mechanism for heat transfer. The inverse capillary number C is also small, however C (or surface tension) multiplies the highest derivative in the water flow equation and so must be retained. Neglecting this term leads to a singular perturbation and a shock will develop in the vicinity of the contact line.

III. ONE-DIMENSIONAL AND APPROXIMATE SOLUTIONS

In order to verify the numerical solutions of the following sections a number of approximations to the governing equations for ice growth and water flow will now be sought. The one-dimensional problem will be tackled first in Sec. III A. In Sec. III B a pseudosteady state solution for the water flow is obtained, this is valid in the bulk. Near the moving front the water moves over a dry surface and the bulk flow solution is inappropriate. In this region the two-dimensional equation may be rescaled, leading to a third-order ordinary differential equation which describes the shape of the moving front. The solution of this equation may be matched to the solution in the bulk flow to completely describe the water height. This is carried out in Sec. III C. Finally, the large time ice accretion and water flow solution is given in Sec. III D.

A. One-dimensional problem

In one-dimension the problem is governed by the mass balance

$$\rho_w \frac{\partial h}{\partial t} = \rho_A W - \rho_i \frac{\partial b}{\partial t} \tag{34}$$

and the energy balance (31). Poots[1] studies a simplified version of (31), which neglects heat conduction through the water layer, so the energy term $q_1 h \equiv 0$ and the ice layer thickness is independent of the water layer thickness. This form of (31) may be integrated immediately. In two and three dimensions, when the driven water film is thin, $q_1 h \ll 1$, this is a reasonable assumption. However, in one dimension $q_1 h$ is typically $\mathcal{O}(1)$ and should be retained. This is demonstrated in Myers and Hammond.[24]

The assumption that $T(0,t) = T_s < T_f$ means that there will always be a period (possibly very short) when all of the incoming fluid turns to rime ice. This is due to the fact that the initial impacting fluid will almost immediately adopt the substrate temperature. Since this is below freezing and there is a nucleation site, the fluid must freeze. Subsequently, water may appear and glaze ice forms. Detailed examination of the early stages of ice accretion on aircraft may show water flowing before ice appears. This typically occurs when the air temperature is relatively high, in which case, air compressibility can lead to above freezing temperatures in the vicinity of the wing. Ice accretion only occurs subsequently, when evaporation of the surface water has cooled the substrate below freezing.

Provided the parameter values are independent of time, initially, the ice thickness is given by (24). When water appears the integrated form of Eq. (34) gives an expression for the water height in terms of the unknown ice thickness:

$$h = \frac{\rho_A}{\rho_w} W(t - t_w) - \frac{\rho_i}{\rho_w}(b - b_w), \tag{35}$$

where b_w and t_w are the ice thickness and time at which water first appears. Equation (35) may be used to replace h in (31), which may then be integrated numerically to determine the ice thickness. Once the ice thickness is known the water thickness and the temperatures in the ice and water can be determined from (35), (26), and (27).

Water first appears when the rime ice temperature reaches the freezing temperature. This is determined from (23), leading to the required expressions for b_w and t_w:

$$b_w = \frac{T_f - T_s}{q_{0r} + q_{1r} T_f} = \frac{\rho_A}{\rho_i} W t_w. \tag{36}$$

This is an exact formula to determine when glaze ice appears. If the denominator is zero, Eq. (36) indicates water will never appear and the accretion will be pure rime ice.

In Myers[22] and Myers and Hammond[24] an experiment on ice accretion in an icing wind tunnel is described. The ice was grown on a model aerofoil. At the end of the experiment a thin slice of the ice was taken. Shining a strong polarized light behind the section revealed the crystal structure and in particular, the transition from rime to glaze. This occurred between 2 and 3 mm. For the same configuration the Fluent v.5 CFD code was run to obtain the air flow, droplet trajectories, and heat transfer coefficients. This provided values for the energy terms q_{0r} and q_{1r}. The theoretical value for the transition [Eq. (36)] was predicted as $b_w = 2.6$ mm. The formula also predicted that glaze ice would never occur below $-16\,^\circ$C, a figure which fits in well with experimental observations. In Myers[22] it is shown that the current method, leads to physically sensible results with a smooth decrease in the freezing fraction (the ratio of mass freezing to that entering the system) from the rime value of unity to the large time value. The standard energy balance used in aircraft icing codes[37] predicts a discontinuity as the freezing fraction jumps from unity to another, lower value. This value is in fact the large time solution of the current model. It was therefore shown that the standard method underpredicts the ice

growth rate and the difference between the current and standard models grows as the temperature increases.

B. Pseudosteady state solution for water flow

Since mass enters the system at a constant rate there exists no true steady-state solution. However, at large times there will exist regions where a quasisteady or pseudosteady state holds in the sense that the bulk water height does not vary. The time dependence enters through the position of the moving boundary.

At large times the two-dimensional water flow far from the edge of the domain is governed by

$$\frac{\partial}{\partial x}\left(\frac{h^3}{3\mu_w}\left(\sigma\frac{\partial^3 h}{\partial x^3}+G_3\frac{\partial h}{\partial x}-G_1\right)+A_1\frac{h^2}{2\mu_w}\right)=\frac{\rho_A}{\rho_w}\beta W. \tag{37}$$

Away from the moving front the water height varies slowly and the surface tension and gravity term in the z direction are negligible. In this region Eq. (37) may be integrated to give

$$\frac{A_1}{2\mu_w}h^2-\frac{G_1}{3\mu_w}h^3\approx\frac{\rho_A}{\rho_w}W\int^x\beta(s)ds+c. \tag{38}$$

The constant of integration is determined by considering the flow in the far field. Depending on the type of flow the film height $h=h_p$ as $x\to+\infty$ or $x\to-\infty$ (h_p is the precursor film height, this is discussed in detail in Sec. IV). For example, if $A_1=0$ and gravity drives the flow in the negative x direction then $h=h_p$ as $x\to+\infty$.

In reality both the catch and air shear must be calculated by an external CFD calculation and provided as model inputs, their values will change as accretion changes and affects the air flow. However, for simplicity, in all of the following numerical examples the air shear is set to a constant value, the incoming fluid is specified by a Gaussian centered on the origin of the coordinate system and constant in time. In two dimensions the catch takes the form

$$\beta=\beta_0\exp(-100\ln(100)x^2)\approx 0.5\exp(-460x^2). \tag{39}$$

The choice of constants in (39) is based on typical aircraft icing values; the coefficient in the exponential means that the catch is at one hundredth of its maximum value 10 cm away from the origin. With this definition for the catch the integral in (38) may be calculated analytically. If the dominant flow is in the negative x direction then

$$\frac{A_1}{2\mu_w}(h^2-h_p^2)-\frac{G_1}{3\mu_w}(h^3-h_p^3)=-\frac{\rho_A\beta_0 W}{\rho_w}\sqrt{\frac{\pi}{4a}}(1-\mathrm{erf}(\sqrt{a}x)), \tag{40}$$

where erf(x) represents the error function. If the dominant flow is in the positive x direction

$$\frac{A_1}{2\mu_w}(h^2-h_p^2)-\frac{G_1}{3\mu_w}(h^3-h_p^3)=\frac{\rho_A\beta_0 W}{\rho_w}\sqrt{\frac{\pi}{4a}}(1+\mathrm{erf}(\sqrt{a}x)). \tag{41}$$

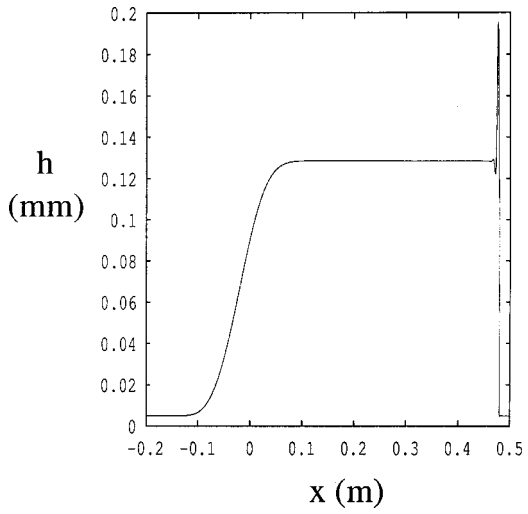

FIG. 2. Global shape of the water layer after 15 s.

So, in general, the height of the fluid away from the front may be determined as the solution of a cubic equation. In the numerical examples of Sec. IV air shear alone drives the flow in the positive x direction. The bulk solution is then determined as the solution of (41) with $G_1=0$. In Fig. 2 a numerical solution of the water flow equation is shown (this is discussed in detail in Sec. IV). The analytical solution given by (41) follows this curve too closely for a difference to be observed on the scale of Fig. 2, hence only the numerical solution is shown. Only near the moving contact line, where surface tension plays an important role and (41) is not appropriate, do the solutions diverge.

C. Film shape in the vicinity of the contact line

Equations (40) and (41) have been derived for two-dimensional flow problems, however, they will also be valid for the three-dimensional examples in the central region where the flow is essentially unidirectional. They provide the solution in the bulk flow but breakdown in the vicinity of the moving contact line. To determine the accuracy of the solutions in this region the method described in Moriarty *et al.*[40] and Tuck and Schwartz[41] is appropriate. Initially the governing equation must be rescaled in the vicinity of the moving front; an appropriate coordinate system which moves with the front is

$$\delta\zeta=x-x_f(t), \tag{42}$$

where $\delta\ll 1$ and $x_f(t)$ is the position of the front. To compare with the results of Sec. IV A, δ is chosen to balance air shear with surface tension and the leading order water height equation becomes

$$\frac{\partial}{\partial\zeta}\left[h^3\frac{\partial^3 h}{\partial\zeta^3}+h^2\right]-\frac{2\mu_w\dot{x}_f}{A_1}\frac{\partial h}{\partial\zeta}=\mathcal{O}(\delta). \tag{43}$$

The speed of the moving front, $\dot{x}_f$, is determined by integrating the two-dimensional film height equation over an interval incorporating the front $x_f\in[x_-,x_+]$. Sufficiently far from the region where fluid enters the system, $\beta\ll 1$, this leads to

$$\int_{x_-}^{x_+} \frac{\partial h}{\partial t} dx + Q_+ - Q_- \approx 0, \tag{44}$$

where Q_-, Q_+ represent the fluid flux at x_-, x_+. Rearranging this expression gives

$$\frac{\partial}{\partial t} \int_{x_-}^{x_+} h \, dx - h_+ \frac{\partial x_+}{\partial t} + h_- \frac{\partial x_-}{\partial t} = Q_- - Q_+ . \tag{45}$$

The height behind the front, h_- is the bulk flow solution determined from either Eq. (40) or (41), ahead of the front $h_+ = h_p$, the precursor film height. Allowing $x_- \to x_f \to x_+$ gives the front velocity,

$$\dot{x}_f \to \frac{Q_- - Q_+}{h_- - h_p}. \tag{46}$$

At leading order, sufficiently far from the front, the general expression for the fluid flux is

$$Q = -\frac{G_1}{3\mu_w} h^3 + \frac{A_1}{2\mu_w} h^2. \tag{47}$$

When air shear dominates the flux, $G_1 \ll A_1$, the speed of the front is

$$\dot{x}_f = \frac{A_1}{2\mu_w}(h_- + h_p). \tag{48}$$

The bulk height is determined from Eq. (41),

$$h_- \approx h_p + \sqrt{\frac{2\mu_w \rho_A \beta_0 W}{A_1 \rho_w}} \sqrt{\frac{\pi}{a}}.$$

The expression for $\dot{x}_f$, Eq. (48), may now be substituted into (43) which may then be integrated immediately. The constant of integration is determined by specifying $h \to h_-$ as $\zeta \to -\infty$. This leads to an ordinary differential equation for the film height

$$\frac{\partial^3 h}{\partial \zeta^3} = -\frac{(h - h_-)(h - h_p)}{h^3}. \tag{49}$$

To solve this equation as an initial value problem the solution in the far field is obtained by perturbing the appropriate height

$$h = h_- + \gamma f(x), \tag{50}$$

where $\gamma \ll 1$. Substituting this into (49) and neglecting terms of $\mathcal{O}(\gamma^2)$ leads to

$$h = h_- + \gamma \exp\left(\frac{\omega}{2}\zeta\right) \cos\left(\frac{\sqrt{3}\omega}{2}\zeta\right), \tag{51}$$

where $\omega^3 = (h_- - h_p)/h_-^3$. Of the three possible solutions for f only one is required in Eq. (51), since one of the two complex roots may be absorbed into an arbitrary choice of origin and the real root gives an unbounded solution as $\zeta \to -\infty$.

Figure 3 shows a close-up of the moving front obtained by the numerical solutions of Sec. IV. Curves (a)–(c) are full numerical solutions of the water height equation using different values for the space step. Curve (d) is the solution of (49) obtained with a fourth-order Runge–Kutta algorithm. The incoming fluid is specified by Eq. (39). All other conditions are given in Table I. Figure 3 is discussed in more detail in Sec. IV A. Curve (d) is used as a reference curve to verify the numerical solutions. Further details on this approach may be found in Moriarty *et al.*[40] and Tuck and Schwartz.[41] An alternative solution method which treats (49) as a boundary value problem is described in Kataoka and Troain.[35,36]

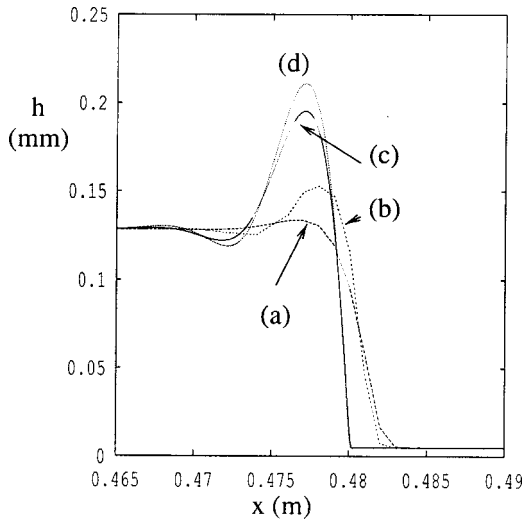

FIG. 3. Comparison of schemes near the moving front (a) upwind scheme, $\Delta x = 10^{-3}$ m, (b) Roe and Sweby superbee, $\Delta x = 10^{-3}$ m, (c) superbee, $\Delta x = 10^{-4}$ m, (d) solution of Eq. (49).

D. Large time ice accretion

At large times there exist two physically realistic possibilities for the ice accretion. A pseudosteady state may exist, where the main body of ice remains at a constant height, sufficiently far from this region the boundary of the accretion moves as a result of the water flow. The second possibility is that ice accumulates for all time. Which of these states is attained depends on the energy terms and whether there is sufficient energy in the system to prevent continual accretion.

If a pseudosteady state exists then the time derivative in (31) tends to zero. The ice thickness is given by

$$b = \frac{k_i(T_f - T_s)(1 - q_1 h)}{k_w(q_0 + q_1 T_f)}. \tag{52}$$

As discussed in Sec. III A, for most cases of practical interest the term $q_1 h \ll 1$ and the final term in the numerator of (52) is negligible. The bulk water height is again determined by the solutions of Sec. III B. If the value of b obtained from (52) is negative, this indicates that there is no physically realistic steady state and ice continues to accrete for all time. In this case the ice thickness is

$$b \approx -\frac{k_w(q_0 + q_1 T_f)}{\rho_i L_f} t. \tag{53}$$

This solution will be valid for ice thicknesses where

$$b \gg \frac{k_i(T_f - T_s)}{k_w(q_0 + q_1 T_f)}, \tag{54}$$

that is, conduction through the ice is negligible. The water height may be obtained by subtracting the ice growth rate, determined by differentiating (53), from Eq. (37) and following through the same analysis of Sec. III B.

A detailed examination of the energy terms shows that under typical aircraft icing conditions ice will continue to grow for all time unless the aircraft velocity is sufficient to raise the local air temperature above freezing. The only other physically realistic option is that the temperature of the incoming droplets is above freezing. This may occur when a cold aircraft moves to a warmer altitude. It is also a common experimental situation where above freezing droplets are sprayed a short distance from the cold surface.

IV. NUMERICAL SCHEMES FOR WATER FLOW

As previously mentioned, the most complex aspect of the current problem is the water flow. In the absence of ice growth the water flow is governed by (16) with $\partial b/\partial t \equiv 0$. Equations of this form have been the subject of intense analytical and numerical study for many years. This form of degenerate equation causes difficulty whenever the film thickness $h \to 0$. In the present problem this will occur in the vicinity of the moving contact line, where the fluid moves over the dry ice surface.

Implicit to the current formulation is a stress singularity at the contact line, due to the no-slip condition being applied at a moving front. To overcome this problem a number of methods may be applied, the two simplest being to employ a Navier slip condition,[42] or to allow a very thin film [typically $\mathcal{O}(10^{-6})$ m] to precede the bulk fluid,[40,43] this is termed a precursor film. The slip condition involves one unknown, the slip coefficient, which must be determined empirically. The value of this coefficient varies, among other things, depending upon the fluid/solid system, the surface roughness and the fluid velocity. Precursor film models also involve one unknown, the precursor film height. Provided this height is chosen correctly, both models give qualitatively similar results.[41] However, the recent analysis of Bowen and King[45] indicates that a slip condition is necessary if a finite contact angle is specified. Without slip the contact angle is zero and a precursor film is required. In the following work a precursor film model will be employed to remove the stress singularity.

A. Two-dimensional water flow scheme

In the absence of ice growth, the two-dimensional equations governing the water flow are

$$\frac{\partial h}{\partial t} + \frac{\partial Q}{\partial x} = \frac{\rho_A}{\rho_w}\beta W, \tag{55}$$

where

$$Q = \frac{h^3}{3\mu_w}\left(\sigma\frac{\partial^3 h}{\partial x^3} + G_3\frac{\partial h}{\partial x} - G_1\right) + A_1\frac{h^2}{2\mu_w}. \tag{56}$$

The numerical scheme employed in this section solves (55) on a regular grid, where Δx denotes the constant space step and Δt the time step. The water height at point i of the grid and at time $t = k\Delta t$ is denoted h_i^k. A typical finite difference scheme in conservative form for Eq. (55) is then[46]

$$h_i^{k+1} = h_i^k - \frac{\Delta t}{\Delta x}(Q_{i+1/2} - Q_{i-1/2}) + \frac{\rho_A}{\rho_w}\beta W \Delta t,$$

where $Q_{i+1/2}$ denotes the flux at the boundary of the i and the $(i+1)$ cells.

Over most of the domain, the dominant term in the flux is the shear stress term, $A_1 h^2/2\mu_w$. If the rest of the flux terms are neglected then (55) is a form of Burgers equation and the solution is likely to develop a shock at the moving contact line. Preventing the shock from developing fully is the surface tension term, $\sigma h^3 \partial^3 h/\partial x^3$, which increases in proportion to the curvature. However, there will still be a region of high curvature at the moving front. In order to accurately describe the front, a simple upwind scheme, which will have strong dissipation, is not adequate. For this reason a flux-limiting method will be employed in the following work.

When calculating the fluxes at the cell boundaries, first-order schemes smooth the solution, second-order accurate schemes tend to create oscillations. A compromise is to balance a second-order accurate scheme with a first-order scheme to provide a smoother solution than with a purely second-order scheme.[47] Hence, at each point, the flux will be computed via

$$Q_{i+1/2} = (1 - c_{i+1/2})Q^{\mathrm{I}}_{i+1/2} + c_{i+1/2}Q^{\mathrm{II}}_{i+1/2}, \tag{57}$$

where $c_{i+1/2}$ is the limiter, Q^{I} and Q^{II} represent the first- and second-order schemes, respectively. The value of $c_{i+1/2}$ varies with the water heights or wave speeds of the neighboring points of the cell. A good choice for the limiter will allow the solution to be second order accurate in the region of the front. In the following work the best scheme is chosen according to its similarity with a limit solution which is calculated with a very small value of Δx and also the solution of the ordinary differential equation described in Sec. III C. A number of tests carried out by the authors indicates that the second order accurate scheme of Roe and Sweby with the so-called ''Superbee'' limiter gives the best approximation of the solution for a reduced number of points.[48–50] In this case, the flux is defined by

$$Q_{i+1/2} = (1 - \phi(r))Q^{\mathrm{UP}}_{i+1/2} + \phi(r)Q^{\mathrm{LW}}_{i+1/2}, \tag{58}$$

where Q^{UP} and Q^{LW} represent the fluxes calculated by upwind and Lax–Wendroff schemes, definitions of a, Q^{UP} and Q^{LW} are given in Appendix B. The limiter $\phi(r)$ is defined by

$$\phi(r) = \max(0, \min(2r, 1), \min(r, 2)),$$

$$r = \frac{(|a_{i+1/2-s}| - \lambda a^2_{i+1/2-s})(h_{i+1-s} - h_{i-s})}{(|a_{i+1/2}| - \lambda a^2_{i+1/2})(h_{i+1} - h_i)},$$

$$s = \mathrm{sign}(a_{i+1/2}).$$

An example of this numerical method is shown in Fig. 2. This depicts a water film on a horizontal surface at time $t = 15$ s. The space step used to obtain this result was Δx

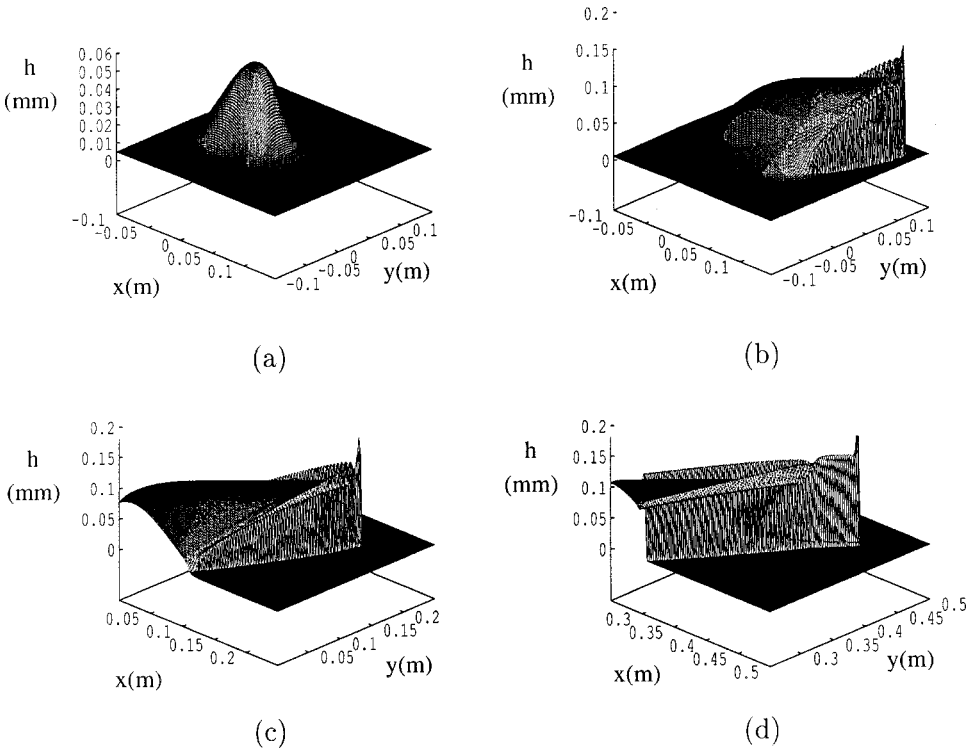

FIG. 4. Three-dimensional water film evolution at times (a) 1 s, (b) 5 s, (c) 7 s, (d) 15 s.

$=10^{-4}$ m, the time step was $\Delta t=10^{-6}$ s. All other parameter values are given in Table I. The incoming fluid is specified by (39).

At the left-hand side of the curve on Fig. 2, the precursor film can be clearly seen. Close to the origin, the height increases, due to the incoming fluid, to approximately 0.13 mm. As x increases, the height remains almost constant for about 0.4 m as all of the incoming fluid flows from left to right under the action of the air shear. At the moving front a capillary ridge, typical of this type of flow, occurs.[35,36,40,41,44,45] After this the fluid readjusts back to the precursor film height. The analytical solution discussed in Sec. III B follows the numerical solution exactly until the capillary ridge. For this reason it is not shown on the figure.

Figure 3 is a close-up of the moving front showing a comparison between the upwind scheme with $\Delta x=10^{-3}$ m, labeled (a), the Roe and Sweby scheme with the Superbee limiter and the same space step, labeled (b), and the Superbee with $\Delta x=10^{-4}$ m labeled (c). The final curve, (d), is the solution to the problem when rescaled in the vicinity of the moving front, as described in Sec. III C, this provides the reference curve. A comparison of curves (a) and (b) shows that the Superbee scheme is best for predicting the capillary ridge for a relatively large space step. The position of the moving front is similar for both curves. Decreasing the space step in the Superbee scheme shows that the solution, represented by curve (c), tends towards the reference curve. Decreasing the space step further increases the correspondence between the numerical solution and curve (d). Out of a number of numerical schemes tested during this investigation, the Superbee was found to provide the most accurate results for a given space step when compared with a reference curve obtained by the method of Sec. III C. This method will be used in all of the following calculations. It is worth noting that there are a number of other numerical methods for solving this form of equation. In particular, the run-time may be significantly reduced by employing an implicit scheme such as that described by Moriarty *et al.*[40] or via a modified ADI method.[52]

B. Three-dimensional water flow

The previous method can be extended to three dimensions. In this case the equation to be solved is (16) with $\partial b/\partial t\equiv 0$. Now the solution space is divided into an $n\times n$ regular grid whose cell sizes are denoted Δx in the x direction and Δy in the y direction. The finite difference scheme in conservative form for the mass balance is written

$$h_{i,j}^{k+1}=h_{i,j}^{k}+\left(\frac{\rho_A}{\rho_w}\beta W-\frac{Q^x_{i+1/2,j}-Q^x_{i-1/2,j}}{\Delta x}-\frac{Q^y_{i,j+1/2}-Q^y_{i,j-1/2}}{\Delta y}\right)\Delta t.$$

The fluxes in the x and y directions Q^x and Q^y are calculated using the same scheme as in the preceding section in each coordinate direction. This means, two wave speeds a^x and a^y and the corresponding parameters r^x and r^y are computed at each point.

Figures 4(a)–4(d) depict the evolution of a water film at times $t=1$, 5, 7, 15 s, ambient conditions are given in Table I. The water film is on a horizontal substrate, with air shear $(A_1,A_2)=(0.5,0.5)$ Pa. The incoming fluid takes the form

$$\beta(x,y)=0.5\exp(-460(x^2+y^2)). \tag{59}$$

The results are computed using the above scheme, with space steps $\Delta x=\Delta y=10^{-3}$ m and the time-step $\Delta t=10^{-4}$ s. Initially the water layer is so thin it is relatively unaffected by the driving forces, which are proportional to h^2 and h^3. Hence, in Fig. 4(a) the fluid resembles the Gaussian source, Eq. (59). As time and the fluid height increases the fluid begins to feel the influence of the driving forces. In Fig. 4(b) the main air shear driven motion leads to a high capillary ridge, there is also a gravity driven spreading producing a smaller ridge to the sides. The side ridges are significantly longer in Fig. 4(c), but the height of the fluid has not changed except at the moving front where a noticeable peak has developed. Since the ambient conditions are the same as for the two-dimensional problem, the height for the bulk fluid is approximately 0.13 mm. Figure 4(d) shows that the leading edge peak breaks free to form a rivulet which moves more rapidly than the bulk fluid. The bulk fluid and rivulet maintain approximately the same height for all times greater than 10 seconds.

V. COMBINED ICE GROWTH AND WATER FLOW

In the following section the numerical method for dealing with water flow is extended to incorporate ice growth. However, before this is done it is first necessary to determine when water appears. As discussed in Sec. III A, there is an initial period when only rime ice forms. In which case the ice thickness is given by Eq. (24). This lasts until time

$$t_w=\min_{x,y}\frac{\rho_i}{\rho_A\beta W}\frac{T_f-T_s}{q_{0r}+q_{1r}T_f}. \tag{60}$$

The ice thickness at this time is $b_w=\rho_A\beta W t_w/\rho_i$. Subsequent to time t_w, water is present in certain parts of the domain, elsewhere the mass balance (24) describes the ice thickness. In the wet region the problem is governed by (16) and (31). However, the extent of the wet domain is not known *a priori*. The method to overcome this problem in two and three dimensions is discussed in the following sections. The three cases presented in this section show typical results from the research program into ice accretion. However, the simulations are carried out under relatively mild temperatures and for longer times than in the pure water flow case of Sec. IV in order to give a reasonable amount of water flow.

A. Two-dimensional ice growth

In the two-dimensional case, the equations to be solved in the wet region are (31) and

$$\frac{\partial h}{\partial t}+\frac{\partial Q}{\partial x}=\frac{\rho_A}{\rho_w}\beta W-\frac{\rho_i}{\rho_w}\frac{\partial b}{\partial t}, \tag{61}$$

where Q is given by Eq. (56). If there is no water on the top of the ice shape, the ice thickness is determined by (24). Denoting the ice height at point i of the grid at time $t=k\Delta t$ by b_i^k, a typical finite difference scheme for Eqs. (31) and (61) is

$$h_i^{k+1}=h_i^k-\frac{\Delta t}{\Delta x}(Q_{i+1/2}-Q_{i-1/2})+\frac{\rho_A}{\rho_w}\beta_i W\Delta t-\frac{1}{\rho_w L_f}\left[k_i\frac{T_f-T_s}{b_i^k}-k_w\frac{q_0+q_1T_f}{1-q_1h_i^k}\right]\Delta t, \tag{62}$$

$$b_i^{k+1}=b_i^k+\frac{1}{\rho_i L_f}\left[k_i\frac{T_f-T_s}{b_i^k}-k_w\frac{q_0+q_1T_f}{1-q_1h_i^k}\right]\Delta t. \tag{63}$$

The effect of gravity on the water flow depends on the angle of inclination of the substrate and the ice shape. As the ice grows, this angle, denoted α, will change. If the angle the substrate makes with the horizontal is denoted α_0 then

$$\alpha=\alpha_0+\arctan\frac{b_{i+1}^k-b_{i-1}^k}{2\Delta x}. \tag{64}$$

This will be used to determine (G_1,G_3) at each time step. In regions where there is no water, the ice height is determined by

$$b_i^{k+1}=b_i^k+\frac{\rho_A}{\rho_i}\beta_i W\Delta t, \tag{65}$$

the water height is fixed at the value of the precursor film h_p.

In order to determine which ice model, rime or glaze, is appropriate at a given point, the following method is used.

(1) The water fluxes are calculated at the boundary of each of the cells.
(2) The water and ice heights are calculated with the glaze ice equations (62) and (63). They require that $b_i^k\neq 0$. For this reason, a precursor ice film b_p is specified (this is set equal to the precursor water film height, 5×10^{-6} m).
(3) If the new calculated water height is greater than the precursor film h_p, then the glaze ice model is taken as correct.
(4) If the new calculated water height is smaller than the precursor film h_p, this means there is no water on top of the ice. The calculated value for the water height is replaced by the precursor film and the new ice height is calculated using Eq. (65).

As the model stands, mass is not conserved. The problem occurs at the rime/glaze interface. At the rime side of the accretion, the flux takes a small constant value (due to the presence of the precursor film). At the glaze side, the flux depends on the height from the neighboring points and so the glaze flux is not necessarily the same as the rime flux. To correct this deficiency, in dry regions, Eq. (65) is modified to

$$b_i^{k+1}=b_i^k+\frac{\rho_A}{\rho_i}\beta_i W\Delta t-\frac{\rho_w}{\rho_i}\frac{Q_{i+1/2}-Q_{i-1/2}}{\Delta x}\Delta t. \tag{66}$$

Since the flux is constant in the precursor film, the new term is only nonzero at the rime/glaze interface. This method ensures continuity and physically sensible results for the water height as well as mass conservation.

In the following example the space and time steps are 10^{-3} m and 10^{-3} s. The explicit form for the energy terms is given in Appendix A, with the ambient conditions specified

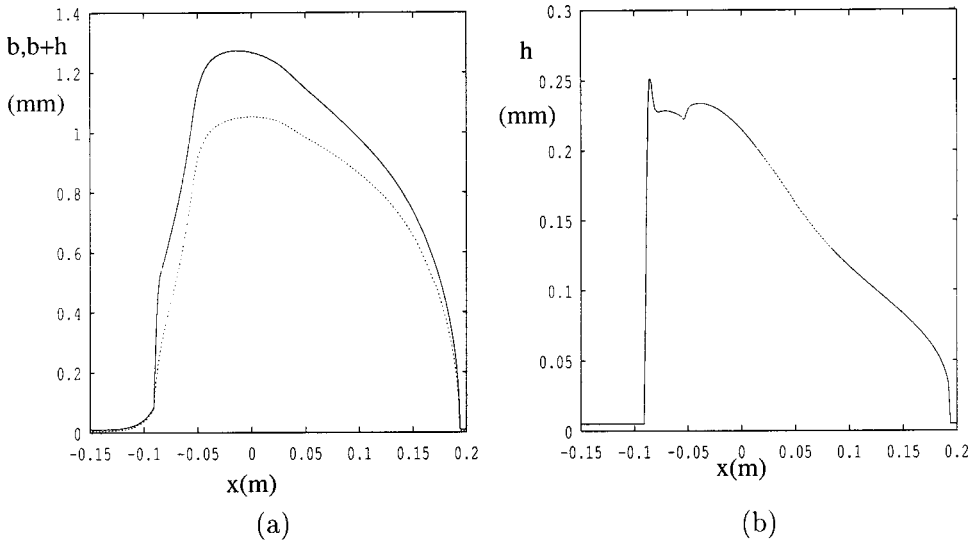

FIG. 5. (a) Two-dimensional ice and water shapes after 60 s, substrate at 20°: the ice is shown as a broken line, the water as a solid line. (b) Two-dimensional water shape after 60 s, substrate at 20°.

in Table I (these are identical to those described in Myers,[22] Myers and Hammond[24]). With the current definition of β, given by (59) the energy terms required for (63) are therefore

$$q_0 \approx 3.49\times 10^5 + 1.01\times 10^5 \exp(-460x^2) \quad \text{K/m}, \tag{67}$$

$$q_1 \approx -1.28\times 10^3 - 3.70\times 10^2 \exp(-460x^2) \quad \text{m}^{-1}. \tag{68}$$

These energy terms correspond to mild icing conditions, with a substrate temperature of 272 K. This high temperature has been deliberately chosen to provide a relatively thick water layer.

Figures 5(a) and 5(b) depict a two-dimensional ice accretion and water layer. The accretion was formed in 60 s on a substrate inclined at 20° to the horizontal and at a temperature of 272 K. Water first appears after 2.06 s. Air shear acts in the positive x direction, against gravity. In Fig. 5(a) the ice is represented by the broken line, the water by a solid line. Note, there is a distinct peak on the ice profile near $x=0$, this is due to the form of β which has a peak at the origin. The ice to the right is caused by the shear induced fluid flow. To the left ice has formed due to the gravity driven flow. The water shape is shown more clearly in Fig. 5(b). A capillary ridge occurs on the left-hand side where gravity drives the flow against the air shear. Between the capillary ridge and $x=-0.05$ is a region where the water height is distinctly different to the smooth shape after $x=-0.05$. In this area the ice curvature is large and so has a significant effect on the flow. The dip in the vicinity of $x=-0.05$ corresponds to a large change in the gradient of the ice, which affects the fluid pressure [see Eq. (12)]. To the right-hand side of the water film the height decreases steadily and there is no capillary ridge. At this side air shear drives the flow against gravity. This absence of a capillary ridge at a moving front has been observed by Kataoka and Troian.[36] Their work deals with the competition between gravity and Marangoni stress. Gravity driven drainage was proposed as the mechanism for preventing the ridge in this case. A constant Marangoni stress leads to exactly the same term in the film height equation as constant air shear. In the present case both gravity and ice accretion act to drain the front. In the example of the following section it is shown that the accretion alone is sufficient to prevent the ridge.

B. Three-dimensional ice growth

The analysis of the preceding section can easily be extended to the three-dimensional case. Equations (62), (65), and (66) become

$$h_{i,j}^{k+1} = h_{i,j}^{k} - \left(\frac{Q^x_{i+1/2,j} - Q^x_{i-1/2,j}}{\Delta x} + \frac{Q^y_{i,j+1/2} - Q^y_{i,j-1/2}}{\Delta y} \right) \Delta t + \frac{\rho_A}{\rho_w} \beta_{i,j} W \Delta t - \frac{1}{\rho_w L_f} \left[k_i \frac{T_f - T_s}{b_i^k} - k_w \frac{q_0 + q_1 T_f}{1 - q_1 h_i^k} \right] \Delta t, \tag{69}$$

$$b_{i,j}^{k+1} = b_{i,j}^{k} + \frac{1}{\rho_w L_f} \left[k_i \frac{T_f - T_s}{b_{i,j}^k} - k_w \frac{q_0 + q_1 T_f}{1 - q_1 h_{i,j}^k} \right] \Delta t, \tag{70}$$

$$b_{i,j}^{k+1} = b_{i,j}^{k} + \frac{\rho_A}{\rho_i} \beta_{i,j} W \Delta t - \frac{\rho_w}{\rho_i} \left(\frac{Q^x_{i+1/2,j} - Q^x_{i-1/2,j}}{\Delta x} + \frac{Q^y_{i,j+1/2} - Q^y_{i,j-1/2}}{\Delta y} \right) \Delta t. \tag{71}$$

In three-dimensions, Eq. (64), which determines the direction of gravity on the ice surface, is replaced by an evaluation of the normal vector on each of the cells. A direct orthogonal basis is $(\mathbf{t_x}, \mathbf{t_y}, \mathbf{n})$, where $\mathbf{t_x}$ and $\mathbf{t_y}$ are unit tangent vectors on the ice surface. The new normal vector $\mathbf{n}'$ is defined as

$$\mathbf{n}' = \frac{-\alpha_1 \mathbf{t_x} - \alpha_2 \mathbf{t_y} + \mathbf{n}}{\sqrt{\alpha_1^2 + \alpha_2^2 + 1}}, \tag{72}$$

where the tangent of the angles is given by

$$\tan \alpha_1 = \frac{b_{i,j+1}^k - b_{i,j-1}^k}{2\Delta y}, \quad \tan \alpha_2 = \frac{b_{i+1,j}^k - b_{i-1,j}^k}{2\Delta x}. \tag{73}$$

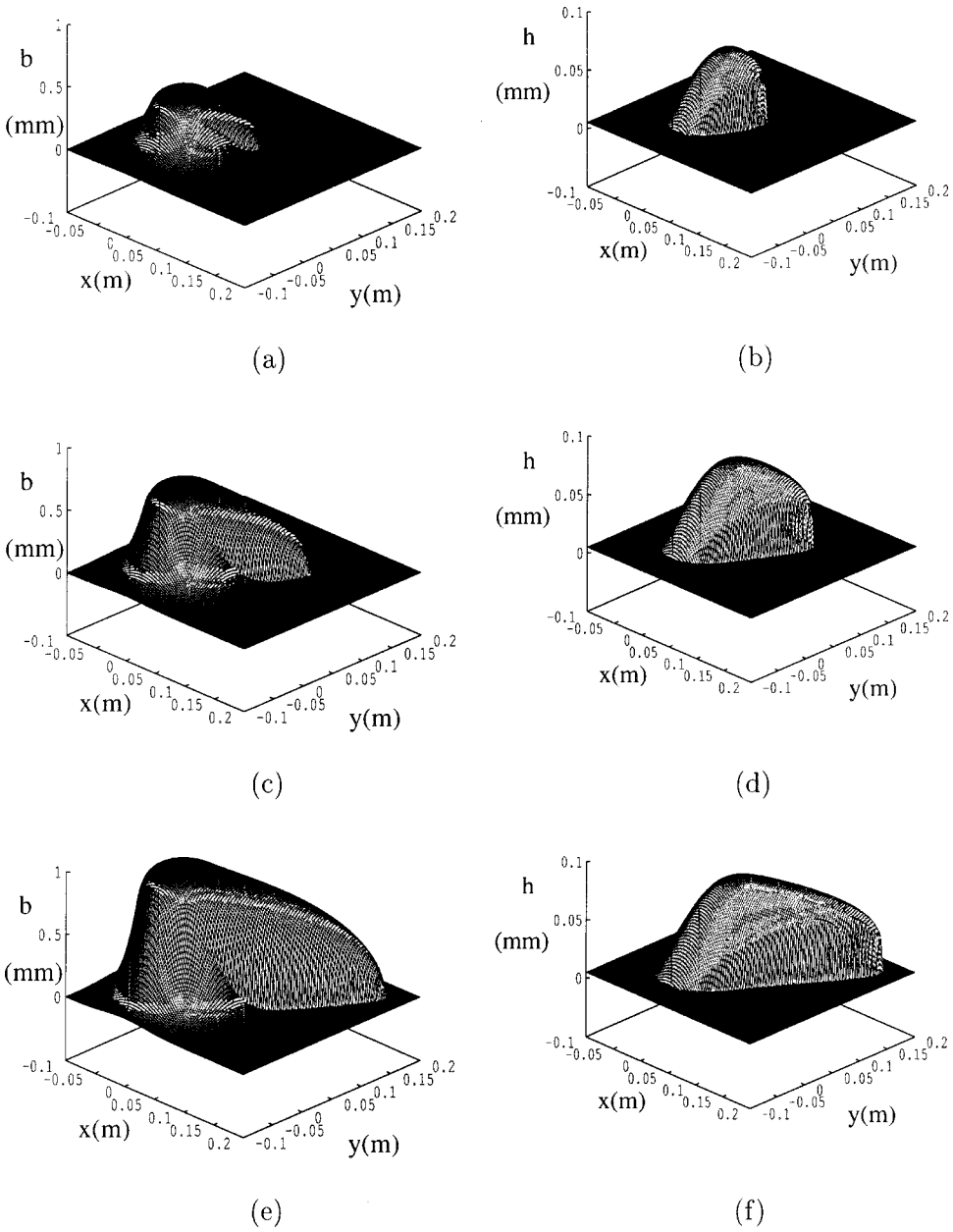

FIG. 6. Three-dimensional ice and water evolution on a horizontal surface: ice shapes after (a) 13.6, (c) 29.1, (e) 60 s; water shapes after (b) 13.6, (d) 29.1, (f) 60 s.

Figures 6(a), 6(c), and 6(e) show the ice shape at $t=13.6$, 29.1, and 60 s for an accretion on a horizontal substrate under the conditions specified in Table I. As in Sec. V A water first appears after 2.06 s. A central Gaussian accretion is clearly visible on Fig. 6(a), with a maximum height of approximately 0.5 mm. A small amount of ice has built up to the right due to the air shear driven flow. In Fig. 6(c), the maximum height is approximately 0.8 mm, the accretion to the right has increased significantly. Figure 6(e) shows the accretion after 60 s. The central peak has increased to a maximum height of approximately 1 mm. The shear driven accretion covers most of the domain to the right of the origin. Figures 6(b), 6(d), and 6(f) show the corresponding water profiles. These figures clearly show that any water above a certain height (in this case approximately 0.08 mm) is blown to the right. At this height the air shear force is sufficient to move the fluid away from the central region. It is interesting to note that a capillary ridge is not present. A thin film driven by a single force will always exhibit a capillary ridge at the moving front, as demonstrated in Fig. 4. The lack of a ridge in the current situation could be explained by the ice accretion term in the water flow equation (69), which acts as a sink for the fluid in much the same way that gravity does on an inclined plane.

Figures 7(a), 7(c), and 7(e) depict an ice accretion under similar conditions to that of Fig. 6, except that now the substrate is inclined at 20° (to act against the air shear). At 13 s after the start of accretion the ice shape is virtually indistinguishable from the previous case. After 29 s the effect of gravity may be observed, with a slight hump appearing on the left-hand side. This hump is clearer after 60 s. The dominant water flow is still to the right, although in Fig. 7(e) the ice does not extend as far as in Fig. 6(e) due to the effect of gravity. In general the ice shapes of Fig. 7 are very similar to those of Fig. 6. The water flow for the two cases is significantly different. Figures 7(b), 7(d), and 7(f) show the water

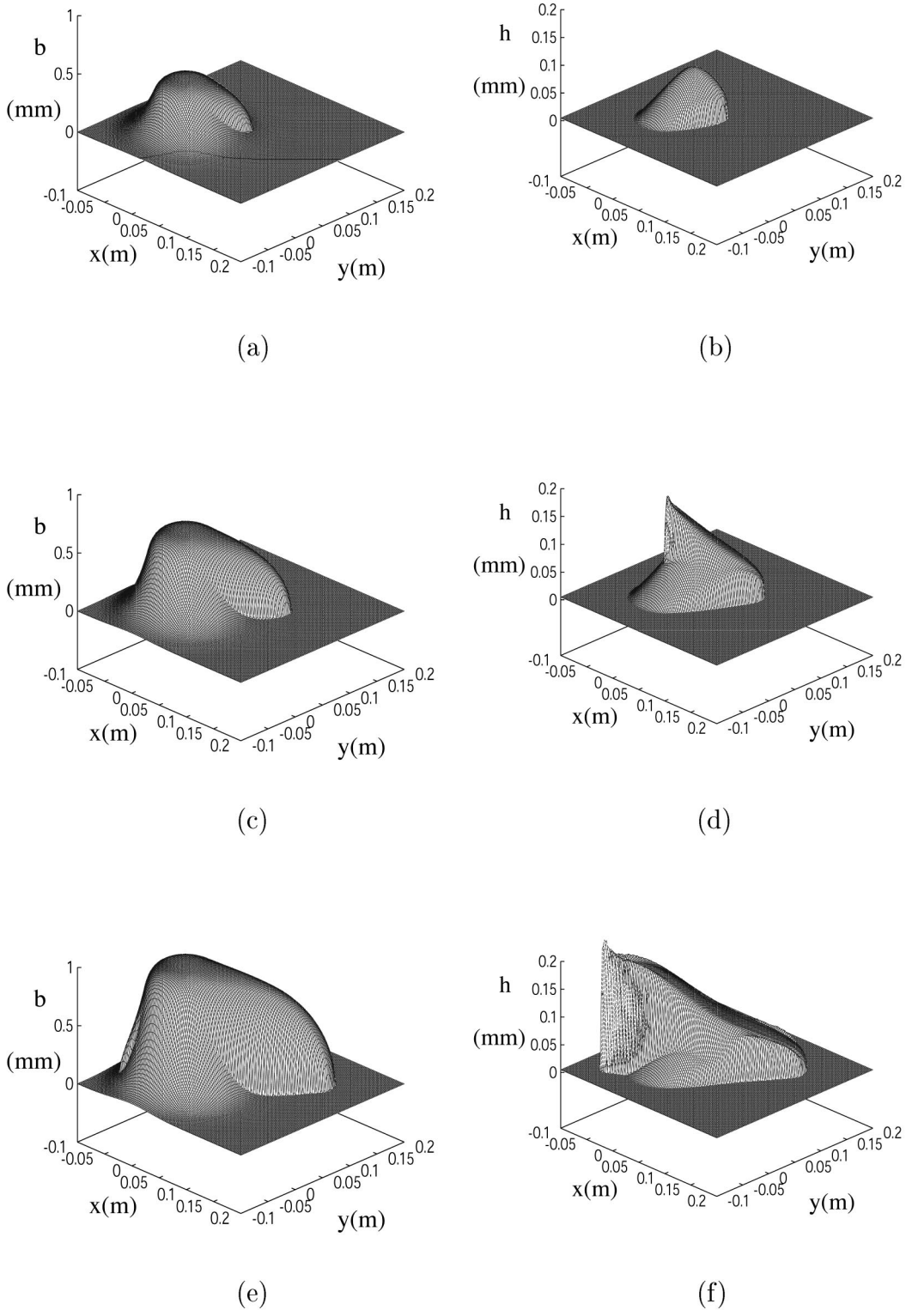

FIG. 7. Three-dimensional ice and water evolution on a surface inclined at 20° for 60 s: ice shapes after (a) 13.6, (c) 29.1, (e) 60 s; water shapes after (b) 13.6, (d) 29.1, (f) 60 s.

shapes corresponding to those of Figs. 6(b), 6(d), and 6(f). The water film depicted in Fig. 7(b) is similar to that of Fig. 6(b) except for the z axis scaling. At this height the water layer is dominated by capillary forces; gravity and air shear have little effect. Subsequently Fig. 7(d) shows that gravity acts to move the fluid to the left against air shear and causes a capillary ridge to develop. The film height in this case reaches a maximum of approximately 0.2 mm. Figure 7(f) shows the water after 60 s, with a much greater spread and a slightly increased maximum height. This highlights the ob-

servation that gravity dominated flow retains a capillary ridge during the accretion process, while air shear dominated flow loses the ridge.

VI. CONCLUSIONS

A mathematical model and numerical technique has been presented to predict ice accretion on a surface at subzero temperatures, due to the impact of a supercooled fluid. The system of interest for the present problem is ice and water, with the flow driven by air shear, gravity, and surface tension. However, the method may be applied to more general solidification problems. The method is not only appropriate for fluids sprayed onto a surface, the liquid may flow through an inlet and subsequently freeze, this will require a change in the model boundary conditions, but the technique remains the same. The air shear driving term is identical to that describing Marangoni driven flow. It is a simple matter to incorporate other forces into the model since, in general, the most difficult aspect of the water flow is the surface tension term which has been dealt with by the current work.

The numerical results for pure water flow show good agreement with the local, approximate solutions and are typical of free surface thin film flows. The Superbee scheme was found to provide the most accurate results for a given space step. The water height quickly approaches a pseudosteady state in the bulk and exhibits a capillary ridge at the moving front. The results indicate that in the absence of freezing the water flow may be well approximated by matching the pseudosteady state and moving front solutions. This approach will be valid for relatively small times. The numerical results for ice accretion are also physically realistic. The water flow on an accreting ice layer has been shown to be significantly different to that over a nonaccreting substrate. Even under the relatively mild conditions investigated, the water height takes a significant time to reach a pseudosteady state, hence the pseudosteady analysis is not valid for practically useful times. The spreading is also retarded as the water nears the cold surface and freezes. When air shear drives the flow the capillary ridge may be absent on an accreting surface. However, in all of the simulations carried out during this investigation a capillary ridge was observed for gravity dominated flows. On a nonaccreting surface a ridge is expected whenever there is a single driving force.

The model developed gives explicit formulas for when the transition from rime to glaze ice occurs and the conditions at which glaze never appears. Previous work has demonstrated that the one-dimensional predictions agree well with experimental work. A version of the method presented in this paper, neglecting the fourth-order surface tension term, is currently being employed in a commercial aircraft icing code, ICECREMO. The validation process is currently ongoing, however, the results so far are very encouraging.

The model requires that the fluid layer is thin, so that the flow may be dealt with by lubrication theory (this is reasonable for all practical applications). The Peclet number must also be sufficiently small so that conduction is the dominant method of heat transfer. The heat equations are then pseudosteady. The physical justification for this pseudosteady behavior is that the heat conduction time scale is rapid compared to the accretion and convection time scales. The temperature therefore has time to equilibrate to an approximately linear profile as the layers slowly accumulate. This places significant restrictions on the flows that may be analyzed in this way. With the current definition of the Peclet number, the physically realistic possibilities for the model to be valid are that the fluid layer is thin and/or the incoming mass rate is low. However, the method is clearly valid for most aircraft icing situations and accretion on structures such as pylons.

A standard approximation concerning the coupling between the air and the thin water film has been employed, namely that the air behaves as if on a solid substrate. In reality, the presence of waves on the film will lead to an increase in drag on the film which will typically augment the fluid velocity and so increase the spreading. This complex problem has not been addressed in the current work. In the numerical examples presented the coupling between the air flow and accreting ice has also not been investigated, although the model will permit solutions with time-dependent input parameters.

The constant air shear term employed in the current code shows that the competition between gravity and air shear may remove the capillary ridge at the moving front. This confirms previous findings for Marangoni driven flow. The results also show that the competition between ice accretion and air shear in the vicinity of the moving front may be sufficient to remove the capillary ridge. However, none of the simulations carried out for this study have shown that ice accretion can remove a capillary ridge produced by gravity dominated flow.

Finally, this work has described the phase change of flowing liquid on a fixed surface. An accretion model specifically designed for rotating systems has also been developed as part of the ICECREMO program. This is applicable to problems in the rotorcraft industry, accretion on a rotating cylinder (which is a standard test for experimental icing conditions in the power industry) and for certain types of spin coating. This model will be described in a later paper.

ACKNOWLEDGMENTS

The ICECREMO project (The Development of 3-D Ice Accretion Modeling) is a collaboration between British Aerospace, Rolls-Royce, GKN-Westland Helicopters Limited, and DERA. The project is managed by the British Aerospace and is in part funded by the DTI under Contract No. RA/6/31/05. The authors would like to thank Dr N. Fowkes of the University of Western Australia for a number of helpful comments.

APPENDIX A: TYPICAL ENERGY TERMS

Typical energy terms for atmospheric icing are as follows:

$$Q_l=\rho_i L_f\frac{\partial b'}{\partial t'},\quad Q_k=\frac{\rho_A\beta W^3}{2}$$

$$Q_d=\rho_A\beta W c_w(T_A'-T_f),\quad Q_h=\overline{H}(T'-T_A),$$

$$Q_a=\frac{r\overline{H}W^2}{2c_a},$$

$$Q_r=\epsilon\sigma_\tau(T'^4-T_A^4)\approx 4\epsilon\sigma_r T_A^3(T'-T_A),$$

$$Q_s=\chi_s(e(T')-e(T_f))\approx\chi_s e_0(T'-T_f),$$

$$Q_e=\chi_e(e(T')-e(T_f))\approx\chi_e e_0(T'-T_f).$$

These represent latent heat, droplet kinetic energy, cooling from incoming droplets, convective heat transfer, aerodynamic heating, radiative heat flux, sublimation, and evaporation, respectively. Primes denote dimensional quantities. It is assumed that the droplets are at the free stream temperature T_A. The convective heat transfer coefficient is denoted $\overline{H}$, r is the local recovery factor, c_a is the specific heat of air, ϵ is the ice surface emissivity, σ_R is the Stefan–Boltzmann constant, χ_s and χ_e are evaporative mass transfer coefficients and $e(T')\approx e_0 T'$ is the saturation vapor pressure.[51] Further details on these energy terms may be found in Refs. 1, 3, 7, 8, 22, 24, 37 and 38.

In the case of rime ice growth, the ice growth rate in Q_l may be equated to $\beta W_{\rho A}$. The boundary condition at the air–ice interface is

$$\begin{aligned}k_i\frac{\partial T'}{\partial z'}&=Q_l+Q_k+Q_a-Q_d-Q_h-Q_r-Q_s\\&=L_f\beta W\rho_A+\frac{\rho_A\beta W^3}{2}+\frac{r\overline{H}W^2}{2c_a}-\rho_A\beta W c_w(T_A\\&\quad-T_f)+\overline{H}T_A+4\epsilon\sigma_r T_A^4+\chi_s e_0 T_f-(\overline{H}\\&\quad+4\epsilon\sigma_r T_A^3+\chi_s e_0)T'.\end{aligned}\tag{A1}$$

This may be expressed in nondimensional form as

$$\frac{\partial T}{\partial z}=q_{0r}+q_{1r}T,\tag{A2}$$

where

$$q_{0r}=\frac{H}{T_f-T_s}\left(\rho_i L_f\beta W\rho_A+\frac{\rho_A\beta W^3}{2}+\frac{r\overline{H}W^2}{2c_a}-\rho_A\beta W(T_A-T_f)+\overline{H}T_A+4\epsilon\sigma_r T_A^4+\chi_s e_0 T_f\right),$$

$$q_{1r}=\frac{H}{T_f-T_s}(\overline{H}+4\epsilon\sigma_r T_A^3+\chi_s e_0),$$

where H is the height scale. This determines Eq. (23).

For glaze ice the boundary condition at the air–water interface is

$$\begin{aligned}k_w\frac{\partial\theta'}{\partial z'}&=Q_k+Q_a-Q_d-Q_h-Q_r-Q_e\\&=\frac{\rho_A\beta W^3}{2}+\frac{r\overline{H}W^2}{2c_a}-\rho_A\beta W(T_A-T_f)+\overline{H}T_A\\&\quad+4\epsilon\sigma_r T_A^4+\chi_e e_0 T_f-(\overline{H}+4\epsilon\sigma_r T_A^3+\chi_e e_0)\theta'.\end{aligned}\tag{A3}$$

The latent heat is produced at the ice–water interface and so does not enter this energy balance. The nondimensional form is

$$\frac{\partial T}{\partial z}=q_0+q_1T,\tag{A4}$$

where

$$q_0=\frac{H}{T_f-T_s}\left(\frac{\rho_A\beta W^3}{2}+\frac{r\overline{H}W^2}{2c_a}-\rho_A\beta W(T_A-T_f)+\overline{H}T_A+4\epsilon\sigma_r T_A^4+\chi e_0 T_f\right),$$

$$q_1=\frac{H}{T_f-T_s}(\overline{H}+4\epsilon\sigma_r T_A^3+\chi e_0).$$

This determines Eq. (22).

APPENDIX B: DEFINITIONS OF WAVE SPEED AND FLUXES

Due to the presence of derivatives in the flux, the usual definition of the quantities necessary to approximate the flux need adapting. At the boundary of the cells, the wave speed $a=\partial Q/\partial h$ is normally computed as follows:

$$a_{i+1/2}=\begin{cases}\dfrac{Q_{i+1}-Q_i}{h_{i+1}-h_i} & \text{if } h_{i+1}-h_i\neq 0,\\ \left.\dfrac{\partial Q}{\partial h}\right|_{i+1/2} & \text{if } h_{i+1}-h_i=0,\end{cases}$$

where Q_i denotes the flux computed at the center of the ith cell of the grid. However, due to the derivatives in the flux, in the present problem the term $\partial Q/\partial h|_{i+1/2}$ is not properly defined. To overcome this the definition of the wave speed is changed to

$$a_{i+1/2}=\begin{cases}\dfrac{Q_{i+1}-Q_i}{h_{i+1}-h_i} & \text{if } h_{i+1}-h_i\neq 0,\\ \left.\dfrac{\partial}{\partial h}\left(\dfrac{G_3}{3\mu_w}h^3+\dfrac{A_1}{2\mu_w}h^2\right)\right|_{i+1/2} & \text{if } h_{i+1}-h_i=0.\end{cases}$$

In the second part of the definition of $a_{i+1/2}$, all the derivatives are set to zero in the flux. Physically, this means that if the water height is constant over two consecutive points, then one assumes that the surroundings of the points are flat in every direction. With the flux reduced to these two terms, it is then possible to express its derivative.

The usual upwind and Lax–Wendroff schemes have the following expressions, see Leveque[46] and Toro:[49]

$$Q_{i+1/2}^{\mathrm{UP}}=\frac{1}{2}(Q_i+Q_{i+1})-\frac{1}{2}\mathrm{sign}(a_{i+1/2})(Q_{i+1}-Q_i),$$

$$Q_{i+1/2}^{\mathrm{LW}}=\frac{1}{2}(Q_i+Q_{i+1})-\frac{\Delta t}{2\Delta x}a_{i+1/2}^2(h_{i+1/2}-h_{i-1/2}).$$

[1] G. I. Poots, *Ice and Snow Accretion on Structures* (Research Studies, Taunton, UK, 1996).
[2] A. E. Davison, ''Dancing conductors,'' AIEE Trans. **49**, 1444 (1930).
[3] L. Makkonen, ''Models for the growth of rime, glaze icicles and wet snow on structures,'' Philos. Trans. R. Soc. London, Ser. A **358**, 2913 (2000).
[4] M. Farzaneh, ''Ice accretions on high-voltage conductors and insulators and related phenomena'' Philos. Trans. R. Soc. London, Ser. A **358**, 2971 (2000).
[5] S. Elliot and G. Warwick, ''Flying on thin ice,'' Flight International 29 April–5 May, 1992.
[6] D. Hughes, ''Safety group highlights CFIT risk for regionals,'' Aviat. Week Space Technol. **140**, 46 (1994).
[7] R. W. Gent, N. P. Dart, and J. T. Cansdale, ''Aircraft icing,'' Philos. Trans. R. Soc. London, Ser. A **358**, 2873 (2000).
[8] E. P. Lozowski, K. Szilder, and L. Makkonen, ''Computer simulation of marine ice accretion,'' Philos. Trans. R. Soc. London, Ser. A **358**, 2811 (2000).
[9] R. W. Gent, ''TRAJICE 2—A combined water droplet trajectory and ice accretion prediction program for aerofoils,'' RAE TR 90054, 1990.
[10] T. Hedde and D. Guffond, ''ONERA three-dimensional icing model,'' AIAA J. **33**, 1038 (1995).
[11] G. A. Ruff and B. M. Berkowitz, ''Users manual for the NASA Lewice Ice Accretion Prediction Code (LEWICE),'' NASA CR 185129, 1990.
[12] Y. Bourgault, H. Beaugendre, and W. G. Habashi, ''Development of a shallow-water icing model in FENSAP-ICE,'' J. Aircr. **37**, 640 (2000).
[13] W. B. Wright, R. W. Gent, and D. Guffond, ''DRA/NASA/ONERA Collaboration on icing research part II-prediction of airfoil ice accretion,'' NASA CR-202349, 1997.
[14] P. Bartlett, ''Development of a new model of ice accretion on aircraft,'' Proceedings of 9th International Workshop on Atmospheric Icing on Structures, Chester, UK, June, 2000.
[15] L. Makkonen and M. Auttti, ''The effects of icing on wind turbines,'' *Wind Energy—Technology and Implementation* (Elsevier Science, New York, 1991), p. 575.
[16] A. C. Fowler, *Mathematical Models in the Applied Sciences* (Cambridge University Press, Cambridge, MA, 1997).
[17] I. A. Frigaard, ''Solidification of spray formed billets,'' J. Eng. Math. **31**, 411 (1997).
[18] E. Gutierrez-Miravete, E. J. Lavernia, G. M. Trapaga, J. Szekely, and N. J. Grant, ''Mathematical model of the spray deposition process,'' Metall. Trans. A **20**, 71 (1989).
[19] J. R. Lister, ''The solidification of buoyancy-driven flow in a flexible-walled channel. Part 1. Constant-volume release,'' J. Fluid Mech. **272**, 21 (1994).
[20] J. R. Lister and P. J. Dellar, ''Solidification of pressure-driven flow in a finite rigid channel with application to volcanic eruptions,'' J. Fluid Mech. **323**, 267 (1996).
[21] A. Defina, ''Two-dimensional shallow flow equations for partially dry areas,'' Water Resour. Res. **36**, 3251 (2000).
[22] T. G. Myers, ''An extension to the Messinger model for aircraft icing,'' AIAA J. **39**, 211 (2001).
[23] T. G. Myers, ''Thin films with high surface tension,'' SIAM Rev. **40**, 441 (1998).
[24] T. G. Myers and D. W. Hammond, ''Ice and water film growth from incoming supercooled droplets,'' Int. J. Heat Mass Transf. **42**, 2233 (1999).
[25] A. L. Bertozzi, ''The mathematics of moving contact lines,'' Notices of the AMS, June/July, 689, 1998.
[26] E. B. Dussan V, ''On the spreading of liquids on solid surfaces: static and dynamic contact lines,'' Annu. Rev. Fluid Mech. **11**, 371 (1979).
[27] K. Stoev, E. Ramè, T. Leonhardt, and S. Garoff, ''The effects of thin films on the hydrodynamics near moving contact lines,'' Phys. Fluids **10**, 1793 (1998).
[28] A. D. D. Craik, ''Wind generated waves in thin liquid films,'' J. Fluid Mech. **26**, 369 (1966).
[29] A. C. King, E. O. Tuck, and J. M. Van den Broeck, ''Air-blown waves on thin viscous sheets,'' Phys. Fluids A **5**, 973 (1993).
[30] J.-C. Tsao, A. P. Rothmayer, and A. I. Ruban, ''Stability of air flow past thin liquid films on airfoils,'' Comput. Fluids **26**, 427 (1997).
[31] C.-S. Yih, ''Wave formation on a liquid layer for de-icing airplane wings,'' J. Fluid Mech. **212**, 41 (1990).
[32] S. Middleman, ''The effect of induced air-flow on the spin coating of viscous liquids,'' J. Appl. Phys. **62**, 2530 (1987).
[33] L. W. Schwartz and D. E. Weidner, ''Modelling of coating flows on curved surfaces,'' J. Eng. Math. **29**, 91 (1995).
[34] D. E. Weidner, L. W. Schwartz, and R. R. Eley, ''Role of surface tension gradients in correcting coating defects in corners,'' J. Colloid Interface Sci. **179**, 66 (1996).
[35] D. E. Kataoka and S. M. Troian, ''A theoretical study of instabilities at the advancing front of thermally driven coating flows,'' J. Colloid Interface Sci. **192**, 350 (1997).
[36] D. E. Kataoka and S. M. Troian, ''Stabilizing the advancing front of thermally driven climbing films,'' J. Colloid Interface Sci. **203**, 335 (1998).
[37] S. K. Thomas, R. P. Cassoni, and C. D. MacArthur, ''Aircraft anti-icing and de-icing techniques and modelling,'' J. Aircr. **33**, 841 (1996).
[38] L. Makkonen, ''A model of icicle growth,'' J. Glaciol. **34**, 1 (1988).
[39] K. Arnold, G. Tetzlaff, and A. Raabe, ''Modelling of ice accretion on a non-rotating cylinder,'' Meterol. Z. **6**, 120 (1997).
[40] J. A. Moriarty, L. W. Schwartz, E. O. Tuck, ''Unsteady spreading of thin liquid films with small surface tension,'' Phys. Fluids A **3**, 733 (1991).
[41] E. O. Tuck and L. W. Schwartz, ''A numerical and asymptotic study of some third-order ordinary differential equations relevant to draining and coating flows,'' SIAM Rev. **32**, 453 (1990).
[42] H. P. Greenspan, ''On the motion of a small viscous droplet that wets a surface,'' J. Fluid Mech. **84**, 125 (1978).
[43] M. A. Spaid and G. M. Homsy, ''Stability of Newtonian and viscoelastic dynamic contact lines,'' Phys. Fluids **8**, 460 (1996).
[44] A. L. Bertozzi and M. P. Brenner, ''Linear stability and transient growth in driven contact lines,'' Phys. Fluids **9**, 530 (1997).
[45] M. Bowen and J. R. King, ''Moving boundary problems and non-uniqueness for the thin film equation,'' Leiden University preprint, MI28-99, 1999.
[46] R. J. LeVeque, *Numerical Methods for Conservation Laws*, Lectures in Mathematics (ETH Zurich, Birkhauser, 1990).
[47] A. Harten, ''High resolution schemes for hyperbolic conservation laws,'' J. Comput. Phys. **135**, 260 (1997).
[48] P. K. Sweby, ''High resolution schemes using flux limiters for hyperbolic conservation laws,'' SIAM (Soc. Ind. Appl. Math.) J. Numer. Anal. **21**, 995 (1984).
[49] E. F. Toro, *Riemann Solvers and Numerical Methods for Fluid Dynamics* (Springer, New York, 1997).
[50] H. Q. Yang and A. J. Przewas, ''A comparative study of advanced shock-capturing schemes applied to Burgers equation,'' J. Comput. Phys. **102**, 139 (1992).
[51] P. R. Lowe, ''An approximating polynomial for the computation of saturation vapor pressure,'' J. Appl. Meteorol. **16**, 100 (1976).
[52] H. M. Eres, D. E. Weidner, and L. W. Schwartz, ''Three dimensional direct numerical simulation of surface-tension-gradient effects on the levelling of an evaporating multi-component fluid,'' Langmuir **1998**, 1859 (1998).